Ni single-atom catalysts for highly efficient electrocatalytic CO_2 reduction: hierarchical porous carbon as a support and plasma modification

Qiulin Ye[a], Yaqi Peng[a*], Dongdong Wang[a], Jiabao Lv[a], Yaoyue Yang[b], Yue Liu[b], Zhifu Qi[c], Songqiang Zhu[c], Chunliang Ge[d], Yan Yang[d], Angjian Wu[a,c *], Shengyong Lu[a*]

Characterization of Ni-SACs/NHPC

The field-emission scanning electron microscopy (SEM, SU-8010, Hitachi), transmission electron microscopy (TEM, Tecnai G2 F20, FEI) and high-angle annular dark-field scanning transmission electron microscope (HAADF-STEM, Themis Z, FEI) were used to investigate the morphology and structure characteristics of the prepared Ni-SA/NHPC catalyst. Brunauer-Emmett-Teller (BET) specific surface area and pore distribution were measured on Kangta Q3 with N_2 adsorption/desorption test. The crystal structure of the catalyst was analyzed by the X-ray powder diffraction (XRD) using Ultima IV with Cu Kαradiation at 3 KW. X-ray photoelectron spectroscopy (XPS) was carried out via Thermo Scientific K-Alpha using Al Kα radiation (1486.6eV). X-ray absorption near edge structure (XANES) and extended X-ray

[a] *State Key Laboratory of Clean Energy Utilization, Zhejiang University, Hangzhou, 310027, P. R. China*
[*] Corresponding author.
E-mail address: pengyaqi@zju.edu.cn, wuaj@zju.edu.cn (A.J. Wu), lushy@zju.edu.cn
[b] *Key Laboratory of Basic Chemistry of the State Ethnic Commission, School of Chemistry and Environment, Southwest Minzu University, Chengdu 610041, Sichuan Province, China*
[c] *Baima Lake Laboratory, Hangzhou, 310053, P. R. China*
[d] *Zhejiang Tiandi Environmental Protection Technology Co., Ltd., Hangzhou 310012, China*

absorption fine structure (EXAFS) of the Ni K-edge were performed at the 1W1B station in Beijing Synchrotron Radiation Facility (BSRF), China, with Ni foil and NiO used as references. The Ni loading weight was measured using inductively coupled plasma mass spectroscopy (ICP-MS, Agilent 7800). Atomic force microscopy (AFM, Dimension Icon, Bruker Nano INC) was carried out to observe the roughness change of carbon substrate treated by plasma. In situ ATR-SEIRAS was measured in a homemade optical setup. It should be ensured that the infrared radiation can penetrate the Si prism into the interface boundary of the Si/Au/IR film at an incidence angle of about 70 °, and then reflect the infrared beam into the liquid nitrogen cooled mercury cadmium telluride detector of the Agilent Cary 660 FTIR spectrometer. High-purity CO_2 was bubbled into the electrolyte at a determined flow rate of about 30 standard cubic centimeters per minute (sccm) to ensure that CO_2 molecules are introduced into the catalyst surface at the same rate. All the spectra were given in absorption units defined as $A = -\log(R/R_0)$, where R and R_0 represent the reflected IR intensities corresponding to the sample- and reference-single beam spectrum, respectively.

Electrochemical CO_2-to CO conversion evaluation in a H-type cell

The electrochemical experiments were performed in a sealed H-cell separated by a Nafion 117 membrane, while the electrocatalytic activity was evaluated using a CHI 760E workstation without iR compensation. The working electrode was prepared by spraying the mixture of Ni-SACs/NHPC, isopropyl alcohol and Nafion solution (5 wt.%) on carbon paper. A platinum foil and Ag/AgCl filled with saturated KCl were used as the counter electrode and reference electrode, respectively. In a typical reaction

process, high-purity CO_2 (99.999%) was continuously purged into the cathodic cell (0.1 M $KHCO_3$ electrolyte) with a set gas flow rate of 30 mL/min. The gas chromatograph (GC, 9790Plus, Fuli) equipped with a thermal conductivity detector (TCD) for H_2 and a flame ionization detector (FID) for CO was used to detect and quantify products after a stable CO_2 electrolysis experiment after 1 h. The liquid products were analyzed by ^1H NMR on a Bruker 600 MHz NMR spectrometer using dimethyl sulphoxide (DMSO) as an internal standard.

All potentials measured by Ag/AgCl electrode were converted to the RHE reference scale using the following equation: $E_{RHE}=E_{Ag/AgCl}+0.0591V \times pH+0.197$ V. The Faradaic efficiency (FE) of various products was calculated as follows:

$$FE(\%) = \frac{anF}{Q} \times 100\% \quad (1)$$

$$j_{CO} = j_{total} \times FE \quad (2)$$

Where a was the number of electrons transferred; n was the number of moles for a given product; F was the Faraday's constant (96485 C/mol); Q was all the charge passed throughout the electrolysis process. j_{total} was the total current density while j_{CO} was the partial current density of CO.

Electrochemical CO_2-to CO conversion evaluation in a flow cell

The electrochemical experiments were conducted in a three-chamber (gas, cathodic and anodic chambers) flow cell. CO_2 electrolysis was conducted under different current densities using CHI 1140e electrochemical workstation. CO_2 was supplied directly to the catalyst layer in the gas compartment while 1M $KHCO_3$ as catholyte and 1M $KHCO_3$ as anolyte were circulated between the corresponding

chamber and the electrolyte supply bottle, respectively, through a peristaltic pump. The CO_2 inlet gas flow rate was controlled using a mass flow controller and set to 30 sccm, and the mixed gas flow rate at the outlet of the reactor was measured using a soap film flow meter. Ag/AgCl filled with saturated KCl as a reference electrode was placed in the catholyte chamber near to the cathode GDE to decrease the solution resistance. The anode GDE was consisted of iridium oxide supported on titanium mesh (IrOx/Ti mesh), prepared by a dip-coating and thermal decomposition method. An anion exchanged membrane (AEM, Fumasep, FAB-PK-130) was adopted to separate the catholyte chamber and anolyte chamber. It should be noted that iR correction was not performed.

DFT simulation

Density functional theory (DFT) calculations were performed on a 3 × 3 × 1 slab model of Ni single-atom catalyst. All the DFT calculations were calculated by using the "Vienna ab initio simulation package" (VASP) using the projector augmented wave(PAW) method with the theoretical basis of density functional theory (DFT)[1]. The slab model was built with 15 Å of vacuum to avoid interlayer interactions and spin polarization was considered. Generalized gradient approximation (GGA) with Perdew, Burke, and Ernzerhof (PBE) was used for the exchange-correlation energy[2]. 3 × 3 × 1 Monkhorst–Pack mesh used for k-point were set in the first Brillouin zone. The cut-off energy for the plane-wave basis was set as 400 eV and a Fermi-level smearing of 0.1 eV. The convergence criteria for total energy and the Hellman-Feynman force were set as 10^{-6} eV and -0.05 eV/Å, respectively. The absorption energy (E_{ads}) was defined as:

$$E_{ads}=E_{slab}+E_{mol}-E_{total} \quad (1)$$

Where the E_{slab} represented the energy of the isolated slab module, E_{mol} represented the energy of isolated molecule, and E_{total}, represented the energy of the species-absorbed system. The reaction can be divided into the following reactions:

$$* + CO_2 \rightarrow *CO_2 \quad (2)$$

$$* CO_2 + (H^+ + e^-) \rightarrow *COOH \quad (3)$$

$$*COOH + (H^+ + e^-) \rightarrow *CO + H_2O \quad (4)$$

$$*CO + H_2O \rightarrow * + CO + H_2O \quad (5)$$

The Gibbs free energy change (ΔG) can be calculated as follows:

$$\Delta G = \Delta E + \Delta ZPE - T\Delta S \quad (6)$$

Where ΔE represented the electronic energy, ΔZPE represented the zero-point energy, T and ΔS represented the temperature (298.15K) and change of entropy calculated by Vaspkit[3].

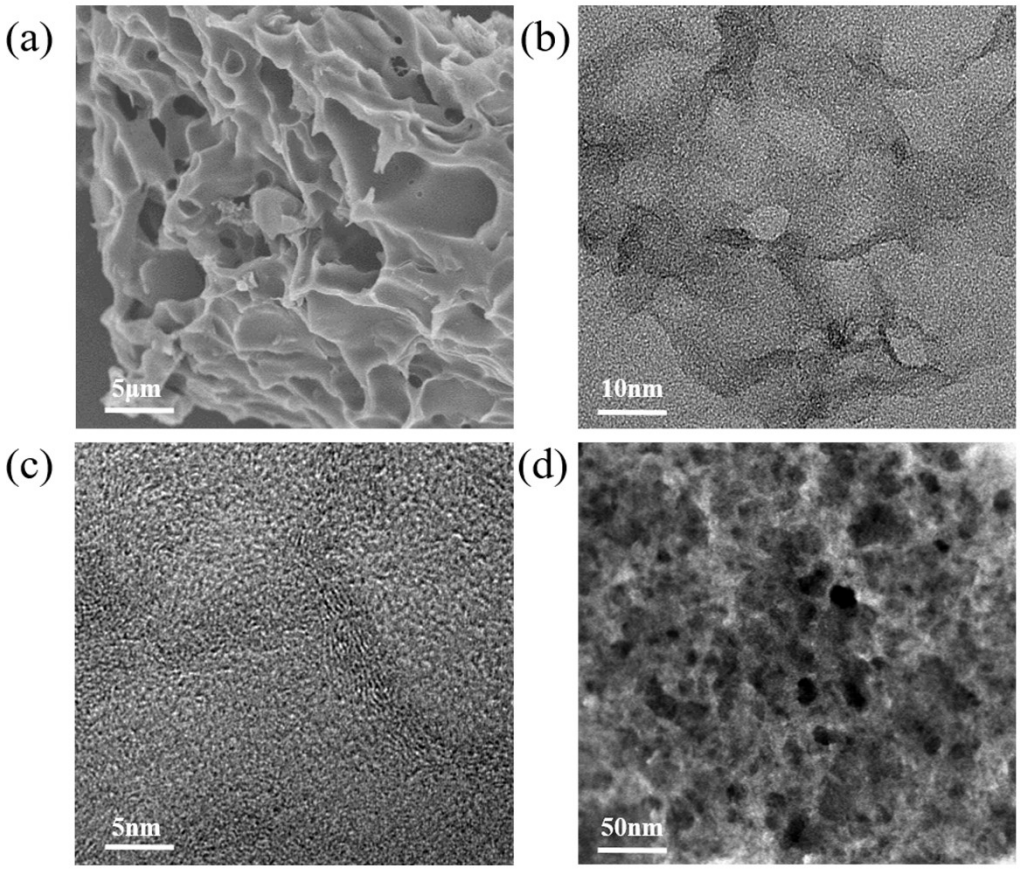

Fig. S1. (a)The SEM, (b)TEM, (c)HRTEM and (d)HAADF-STEM images of the Ni-SACs/NHPC.

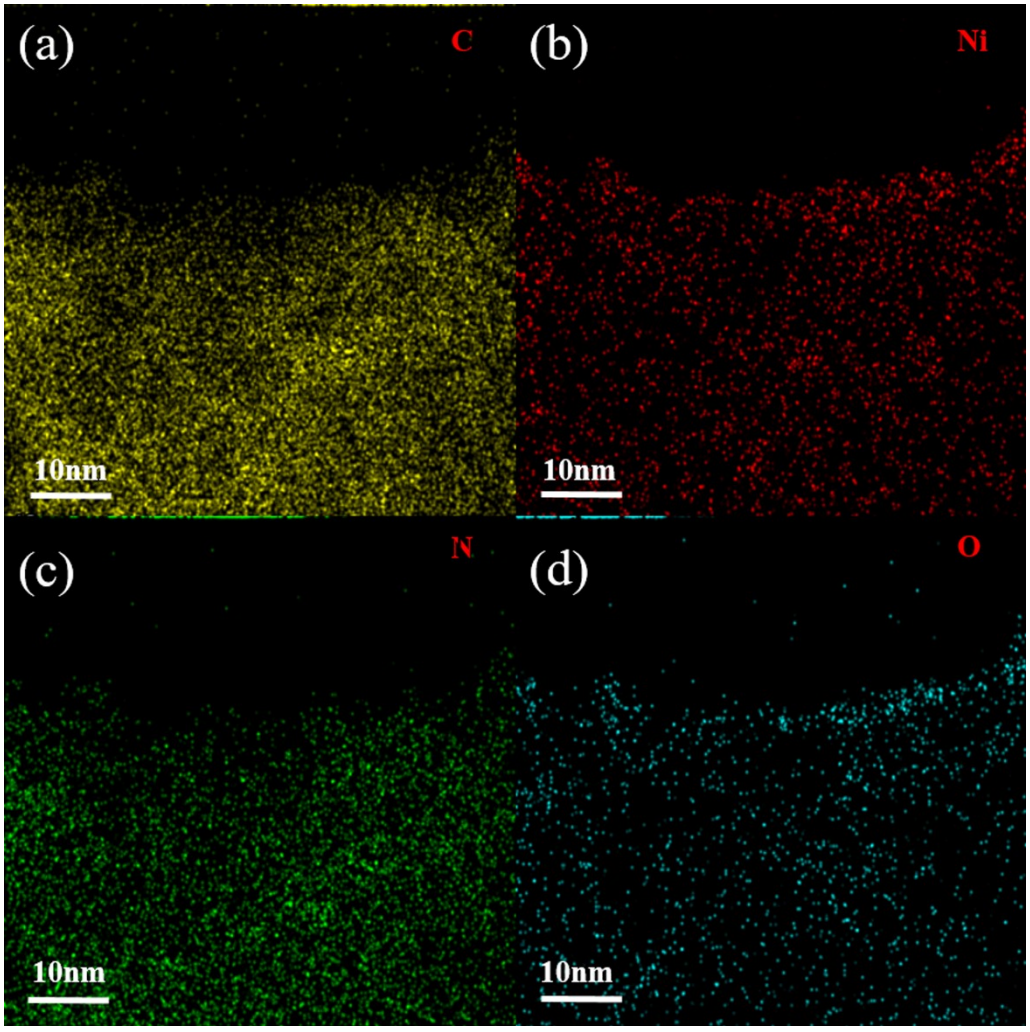

Fig. S2. The corresponding EDS mapping of Ni-SACs/NHPC.

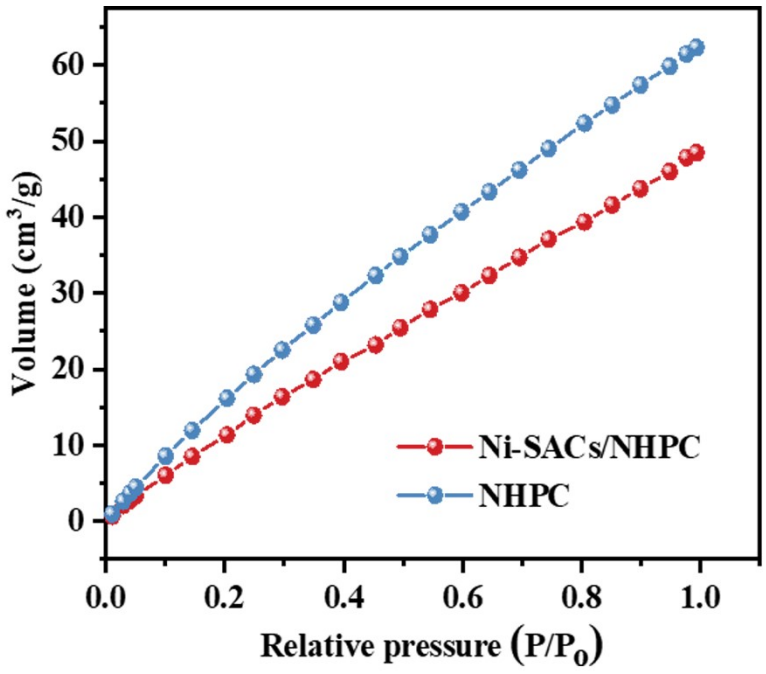

Fig. S3. CO_2 adsorption isotherm for Ni-SACs/NHPC.

Table S1. BET characterization. BET surface area, surface area of micropore (S_{micro}), surface area of mesopore (S_{meso}) and total pore volume of NHPC and Ni-SACs/NHPC.

Sample	S_{BET} (m^2/g)	S_{micro} (m^2/g)	S_{meso} (m^2/g)	Total pore volume (cm^3/g)
NHPC	2115.7	1581.3	534.4	1.08
Ni-SACs/NHPC	1115.6	1001.3	114.3	0.643

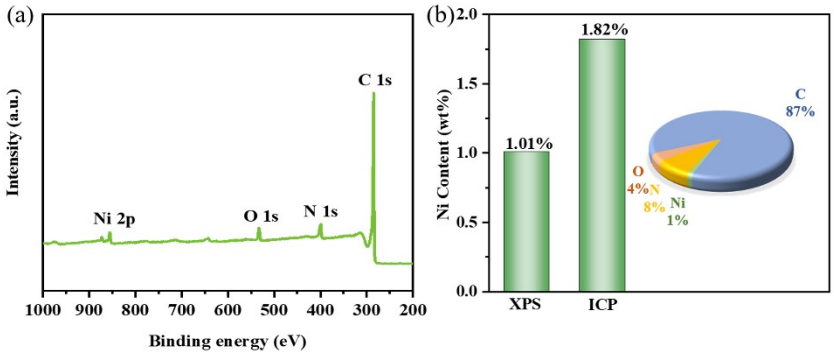

Fig. S4. (a)The survey XPS spectra for Ni-SACs/NHPC; (b)Ni content of Ni-

SACs/NHPC from XPS and ICP measurements.

Table S2. The parameters for subpeaks in Fig. 2(c).

Samples	Subpeaks	Position (eV)	Amount (%)
Ni-SACs/NHPC	C-C	284.75	21.15
	C-N	285.00	31.07
	C-O	285.84	26.10
	C=O	288.94	21.68

Table S3. The parameters for subpeaks in Fig. 2(b).

Samples	Subpeaks	Position (eV)	Amount (%)
Ni-SACs/NHPC	Pyridinic-N	398.51	20.54
	Ni-N	399.27	24.46
	Pyrrolic-N	400.86	30.83
	Graphite-N	401.75	14.35
	Oxidized-N	404.50	9.82

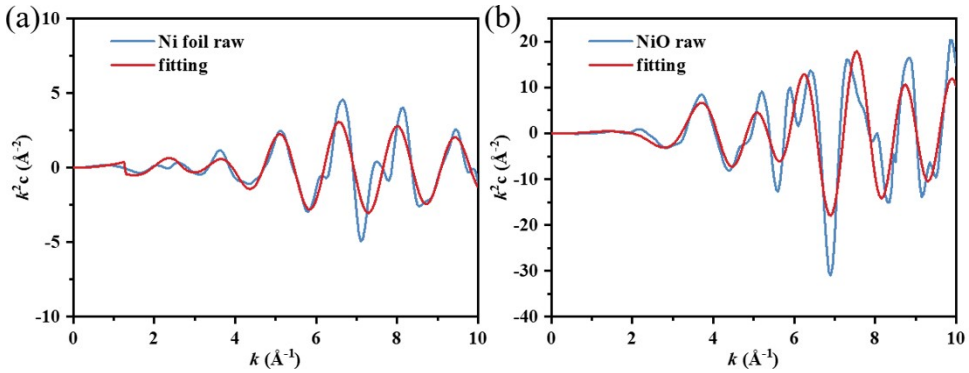

Fig. S5. The EXAFS fitting in K-space for (a)Ni-foil; (b)NiO.

Table S4. EXAFS fitting parameters at the Ni k-edge various samples(S_0^2=0.82)

Sample	Path	C.N.[a]	R (Å) [b]	σ (×10^{-3}Å^2) [c]	ΔE (eV) [d]	R factor[e]
Ni-foil	Ni-Ni	12*	2.49*	6.0±2.0	6.4±0.2	0.001
NiO	Ni-O	6*	2.11*	4.6±1.7	5.7±1.7	0.005
	Ni-Ni	12*	2.98*	6.8±0.7		
Ni-SACs/NHPC	Ni-N	3.9±1.2	1.86±0.03	9.0±6.0	-8.9±5.3	0.033

[a]C. N.: coordination numbers;

[b]R: bond distance;

[c]σ^2: Debye-Waller factors;

[d]ΔE_0: the inner potential correction.

[e]R factor: goodness of fit.

*The experimental EXAFS fit by fixing C. N. as the known crystallographic value.

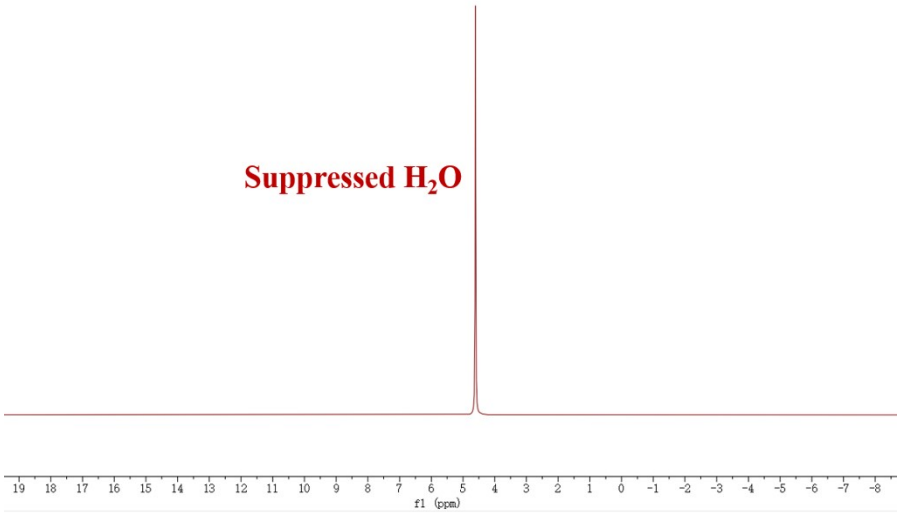

Fig. S6. NMR spectra of the electrolyte after CO_2 reduction electrolysis of 9h at potentials of -0.94 V vs.RHE for the Ni-SACs/NHPC.

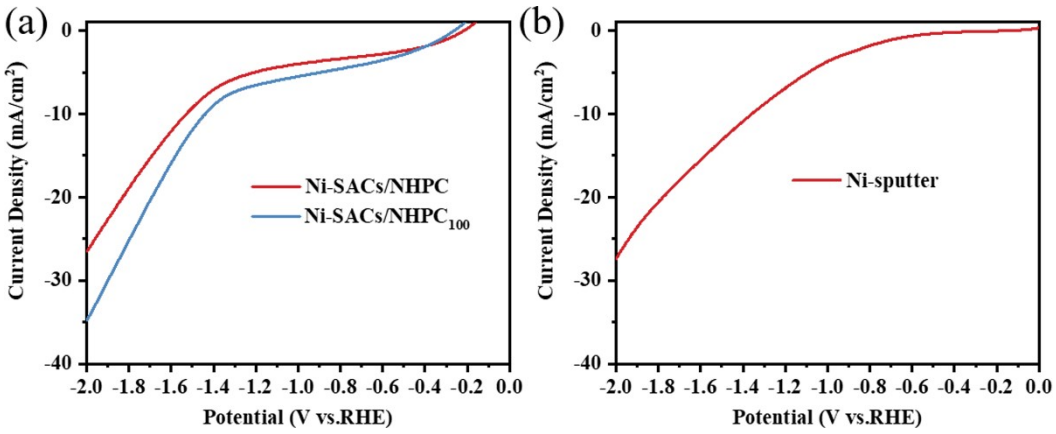

Fig. S7. The linear sweep voltammetric (LSV) curves of (a)Ni-SACs/NHPC and Ni-SACs/NHPC$_{100}$; (b)Ni-sputter in CO_2-saturated 0.1M $KHCO_3$ electrolyte at a scan rate of 50 mV/s, respectively.

Table S5 Comparisons of the catalytical performance towards CO production using Ni based single atom catalysts in the H-type cell

Catalyst	Electrolyte	Potential (vs. RHE)	FE_{CO} (%)	J_{CO} (mA cm^{-2})	References
Ni-SACs/NHPC	0.1M $KHCO_3$	-1.04V	98.25	14.97	this work
PCN-222(Ni)/CNT	0.5M $KHCO_3$	-0.8V	52	0.8	4
Ni/NC	0.1M $KHCO_3$	-0.8V	92.3	4.6	5
Ni/N-C	0.5M $KHCO_3$	-0.8V	91.1	16.2	6
Ni-NC_ATPA@C	0.5M $KHCO_3$	-0.7V	93.7	7	7
Ni-N-C	0.1M $KHCO_3$	-0.9V	94.6	10.5	8

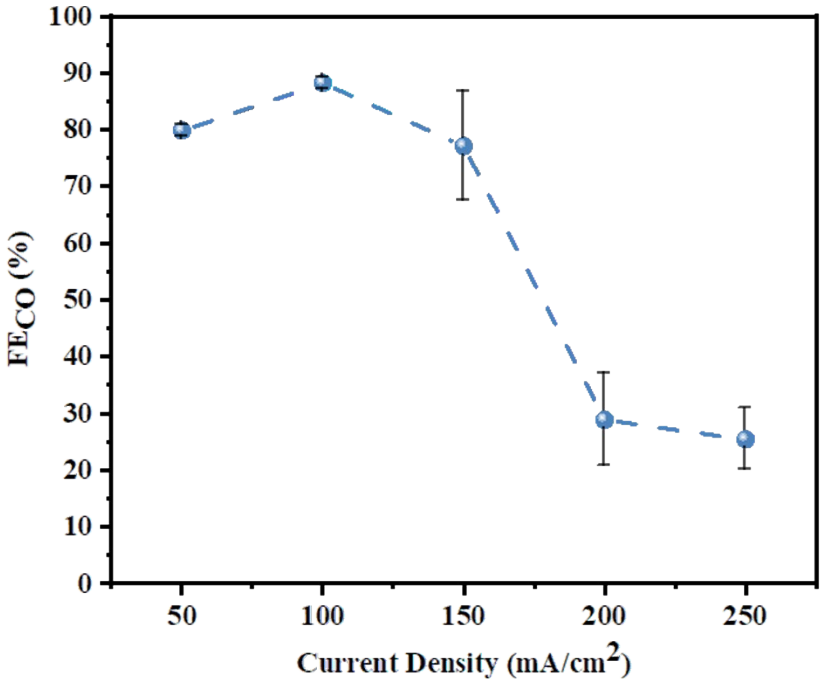

Fig. S8. CO Faraday efficiency of Ni-SACs/NHPC at different current densities in a flow cell system

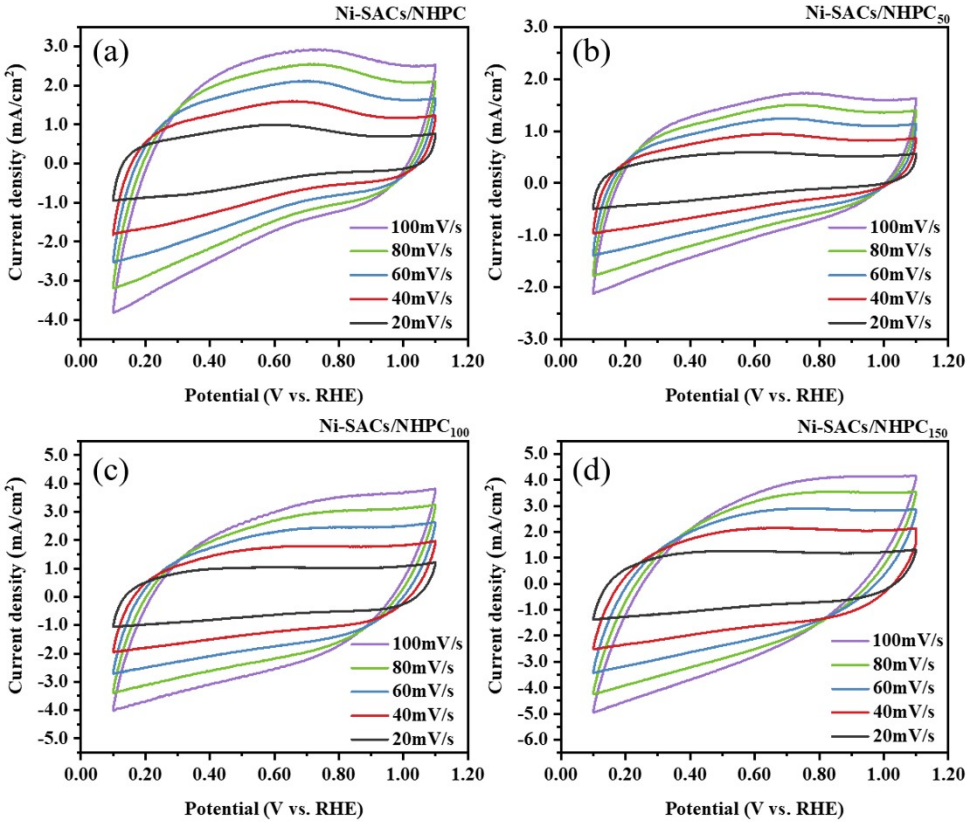

Fig. S9. Cyclic voltammetry measurements for Ni-SACs/NHPC, Ni-SACs/NHPC$_{50}$, Ni-SACs/NHPC$_{100}$ and Ni-SACs/NHPC$_{150}$ performed at different scan rates e.g., 20, 40, 60, 80, and 100 mV/s.

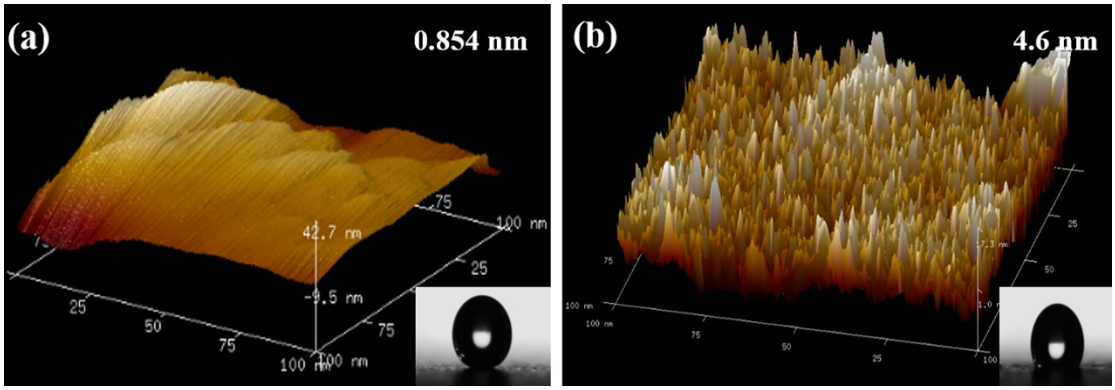

Fig. S10. Comparisons of AFM images and contact angle measurements of carbon substrate without (a) and with plasma treatment (b).

1 G. Kresse, J. Furthmüller.Physical Review B, 1996, 54.

2 John, P., Perdew.Physical Review Letters, 1996, 77(3865-3868.

3 V. Wang, N. Xu, J.C. Liu.2019, 108033.

4 M. Liu, M. Peng, B. Dong.Chinese Journal of Structural Chemistry, 2022, 41(7): 2207046-2207052.

5 F. Li, S. Hong, T.-S. Wu. ACS Applied Energy Materials, 2019, 2(12): 8836-8842.

6 S.-J. Zheng, H. Cheng, J. Yu.Rare Metals, 2023, 42(6): 1800-1807.

7 M.W. Jia, C. Choi, T.S. Wu.Chemical Science, 2018, 9(47): 8775-8780.

8 X.X. Huang, Y.J. Ma, L.J. Zhi.Acta Physico-Chimica Sinica, 2022, 38(2).